

**MODELLING OF THE INFLUENCE
OF ELECTROMAGNETIC FORCE ON MELT
CONVECTION AND DOPANT DISTRIBUTION
AT FLOATING ZONE GROWTH OF SILICON**

A. Sabanskis¹, K. Surovovs^{1,2}, A. Krauze¹, M. Plāte¹, J. Virbulis¹

¹ *Faculty of Physics and Mathematics, University of Latvia,
8 Zellu str., LV-1002, Riga, Latvia*

² *Institute of Solid State Physics, University of Latvia,
Kengaraga str. 8, LV-1063, Riga, Latvia
e-Mail: kirils.surovovs@lu.lv*

Numerical modelling of the floating zone process is considered. A local analysis of the electromagnetic field distribution in the vicinity of the external triple point was carried out using the complex vector potential formulation, and the result was included in the calculation of phase boundaries to improve the surface current formulation. 3D hydrodynamic calculations were performed using the open source code library OpenFOAM. The influence of a high-frequency electromagnetic field is shown by comparing phase boundaries, convection in melt and radial resistivity variation profiles. Results are compared with experimental data.

Introduction. There are two main methods to grow silicon single crystals for microelectronics: the Czochralski (CZ) method and the floating zone (FZ) method. Crystals grown by the CZ method have a relatively high dopant concentration due to the contact between the silicon melt and a quartz crucible. On the other hand, the FZ process is appropriate for power electronics (high purity crystals), because molten silicon is not in contact with other materials.

In the FZ method, a high-frequency (HF) inductor is used to melt a polycrystalline silicon feed rod. It induces currents in the silicon (see Fig. 1, left) that flows only in a thin skin layer due to the high frequency of alternating inductor current, typically of about 3 MHz. Being pulled by gravity, the molten silicon flows downwards through the hole in the middle of the inductor and forms a large droplet due to a relatively high surface tension.

At some distance below the inductor, where the induced electromagnetic (EM) power is lower, the molten silicon crystallizes due to radiative heat losses. It forms a single crystal, because the characteristic velocities of this process are very low – several millimetres per minute. The FZ method is realized in the atmosphere of noble gases (usually argon). Before the 1980s of the XX century, only small diameter crystals had been grown, but the needle-eye technique, in which the crystal radii and the feed rod are much greater than the inner radius of an induction coil (see Fig. 1, right) allowed to reach even 200 mm diameter. This is more convenient for industrial purposes, because many elements can be created and etched on a single wafer (i.e. on a thin silicon disc), but the growth process becomes more complicated for bigger crystal diameters.

To develop the FZ process, numerical modelling can be used. Its advantages are inexpensiveness and possibility to reveal some aspects that cannot be observed directly, e.g., hydrodynamics in the melt. It is crucial to describe the EM field as precisely as possible, because it influences the shape of phase boundaries as well as

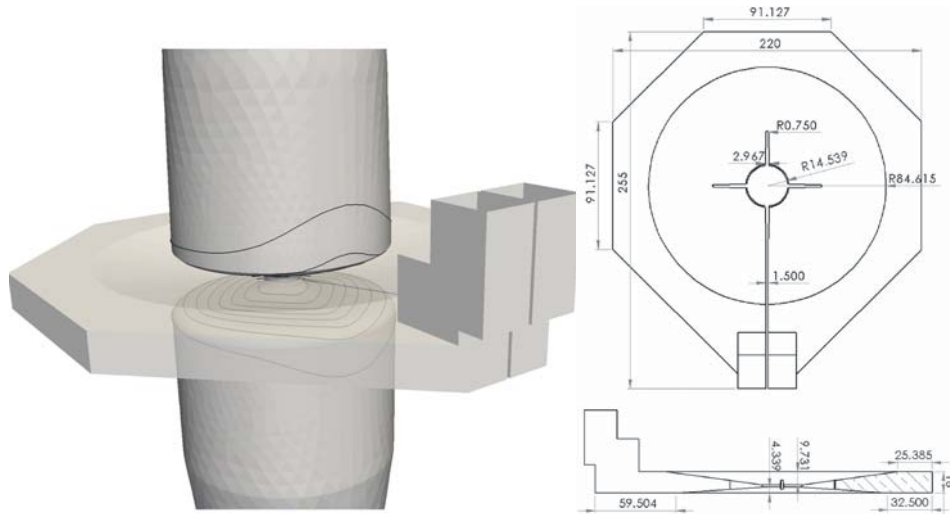


Fig. 1. Left: overall view of a 3D model of the FZ system: feed rod, melt and crystal with current lines, and HF inductor. Right: drawings of the inductor (top and side views).

convection and dopant transport in the melt. From the dopant field, it is possible to obtain radial resistivity variation (RRV) in the grown single crystal [1]. This result is important for industrial crystal growing companies which are interested to produce better crystals, i.e. crystals with more homogeneous resistivity profiles.

It is possible to improve and verify the existing FZ models using new available experimental data. In the present work, the EM correction is introduced and verified by comparison with experiment. The influence of the electromagnetic field on phase boundaries, melt convection and dopant distribution in the melt is shown and discussed. Main physical fields in the melt are analyzed, the shape of the crystallization interface and RRV profiles are compared with experimental data obtained from the Institute for Crystal Growth, Berlin [2].

1. Mathematical models and software.

1.1. Phase boundaries. 2D axisymmetric calculations of phase boundaries were carried out using a specialized program FZone [3]. Since the skin depth varies between 0.038 mm for the copper inductor and 1.3 mm for solid silicon and is much less than the characteristic dimensions of the FZ system (≈ 0.1 m), the EM field distribution is determined by the surface current density. A HF EM field is calculated considering the 3D HF inductor [4]. 3D induced EM surface power density distribution is azimuthally averaged and included in 2D axisymmetric phase boundary calculations as heat sources. Diffusive thermal radiation is taken into account using the axially symmetrical view factor model, assuming all surfaces optically grey and opaque, with temperature-dependent emissivity. From the calculated temperature field and heat flux densities at the interfaces, the direction and the magnitude of the movement of each interface point are obtained, and the quasi-stationary shape of phase boundaries is found iteratively. The free surface shape is found considering the hydrostatical pressure, electromagnetic pressure, surface tension and the centrifugal force. To obtain an open melting front shape, a thin fluid film model is used, assuming that the feed rod melting is axially symmetrical [3].

1.2. EM correction. The HF approximation, which is described in [3], cannot be used when the exact distribution of volumetric EM field is important,

for example, in the vicinity of the solid-liquid interface, where the skin depth changes by a factor of five. A local analysis of the EM field distribution in the vicinity of the external triple point (ETP) (the point position is shown in Fig. 3) was carried out using the complex vector potential formulation. The internal triple point (ITP, its position is shown in Fig. 3) was not considered due to the presence of a thin melt film on the open front that has the same conductivity as the whole melt and, therefore, the EM field distribution is not changed there so dramatically.

A small domain near the ETP was considered. For the radial domain, a size much smaller than the crystal radius curvature in the azimuthal direction can be neglected and a 2D approximation can be used. Therefore, all currents are passing perpendicular to the xz (vertical) plane and the vector potential has only one component A_y . The following equation was numerically solved:

$$\Delta A_y - i\omega\sigma\mu A_y = 0,$$

where A_y is the azimuthal component of the complex vector potential, i is the imaginary unit, $\omega = 2\pi \cdot 3 \text{ MHz}$ is the inductor current angular frequency, σ is the silicon conductivity ($5 \cdot 10^4 \text{ S/m}$ for solid and $1.2 \cdot 10^6 \text{ S/m}$ for liquid) and $\mu = 4\pi \cdot 10^{-7} \text{ N/A}^2$ is the magnetic constant. Boundary conditions were (see Fig. 2, left):

- a. $A_y = 0$ at the left boundary of the calculation domain;
- b. $A_y = 1$ at the right boundary of the calculation domain (modelling the presence of an inductor with a fixed current that passes in the y -direction);

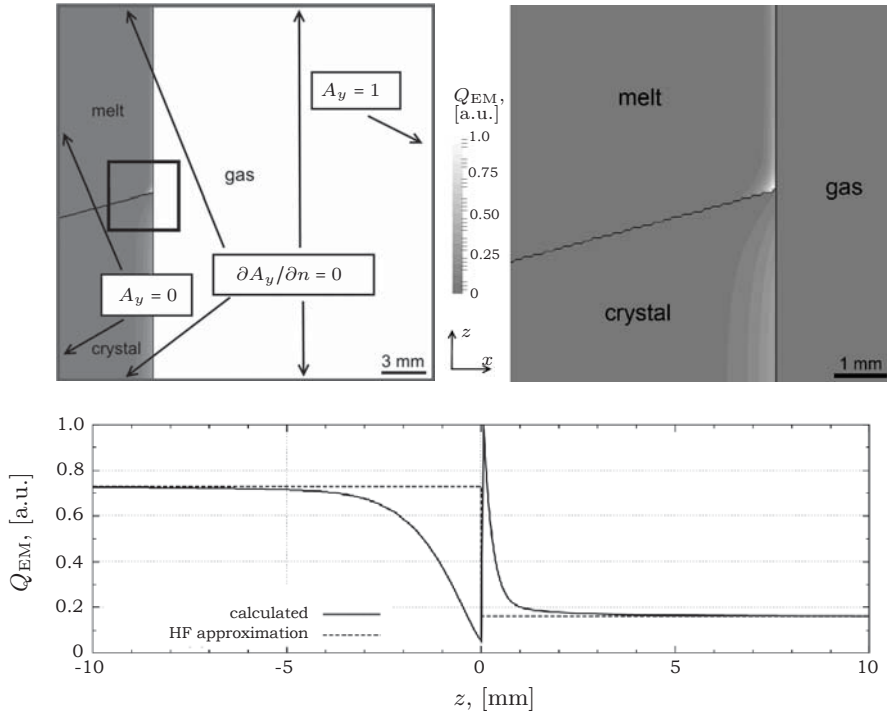


Fig. 2. Top left: the entire calculation domain with boundary conditions for vector potential. Top right: the induced EM power density distribution in the vicinity of ETP (shown by the square on the left image), arbitrary units. Bottom: linear induced EM power as a function of the vertical coordinate in the melt ($z > 0$) and in the crystal ($z < 0$), arbitrary units. Solid line shows the result calculated with the vector potential formulation and dashed line – previously used HF approximation.

c. $\partial A_y / \partial n = 0$ at the top and bottom boundaries of the calculation domain (symmetry conditions).

The equation was solved by the finite difference method on a rectangular grid. The calculation domain of $24 \times 24 \text{ mm}^2$ was divided in 400×400 points. It was obtained that in the first few millimetres near the ETP the actual induced EM power was significantly different from the induced EM power far from the ETP (and thus different from the imprecise power distribution previously obtained by the HF approximation). More power is induced in the melt and less in the crystal (see Fig. 2, top right). By integrating the heat distribution along lines parallel to the crystal-melt interface, a surface heat source density distribution is obtained (see Fig. 2, bottom).

The result of local analysis was included in FZone as a correction to EM heat sources at free melt and crystal side surfaces. This correction was used only in axially symmetric calculation of phase boundaries as a correction to the boundary conditions for temperature, not directly in 3D HF EM calculations. Because of the changed EM heat sources in the crystal and in the melt, the inductor current needs to be adjusted to maintain the same zone height. The crystallization interface shape near the ETP changes due to the change of local heat sources; the change of shapes on global scale occurs due to a different inductor current and integral induced power on the melt free surface.

1.3. 3D melt flow. The unsteady 3D melt flow in the FZ process is modelled using the open source code library OpenFOAM. For the considered system, the Reynolds number is roughly 1500, therefore, the melt flow is considered laminar. The detailed description of the mathematical model is given in [1]; only the details relevant to the present study are summarized.

For an incompressible melt flow, the Navier-Stokes equations are solved, and for the description of buoyancy, the Boussinesq approximation is used. Boundary conditions for the melt velocity are:

a. The crystallization interface is considered as a velocity outlet including constant mass outflow and crystal rotation.

b. The melting interface is considered as an inlet and the desired mass inflow is set equal to the outflow through the crystallization interface. A ring-shaped profile is used for the vertical velocity component to simulate the melt flow from the open melting front through the thin melt film.

c. The distribution of the Marangoni surface force (obtained from the temperature field recalculated at every time step) and the EM surface force distribution (acquired from the 3D HF EM calculations) are used to set boundary conditions for the melt velocity on the melt free surface:

$$f_s = \frac{1}{4} \mu \delta \nabla j^2 + M \nabla T,$$

where f_s is the surface force,

$$\delta = \frac{1}{\sqrt{\pi f_{\text{ind}} \sigma \mu_0}}$$

is the skin depth, ∇ is the surface gradient, j is the surface current density, $M = -1.3 \cdot 10^{-4} \text{ N/(mK)}$ is the Marangoni coefficient, T is the temperature, f_{ind} is the inductor current frequency, and σ is the conductivity of liquid silicon. The Marangoni force is directed from higher to lower temperatures, whereas the EM force F_{EM} is typically in the opposite direction.

The temperature field is governed by the non-stationary convection-diffusion equation. The corresponding boundary conditions are the following:

a. Fixed temperature equal to the melting point of silicon (1687K) at the melting and crystallization interfaces.

b. Fixed heat flux density equal to the sum of radiative heat losses (negative) approximated from axially symmetrical FZone [3] calculations and induced EM power density on the melt free surface.

For the dopant concentration field C , the mass transport equation is solved. From the calculated C distribution at the crystallization interface the resistivity of the grown crystal ρ can be obtained: $\rho = 1/(k_0C)$, where $k_0 = 0.35$ is the segregation coefficient. The boundary conditions are:

a. At the crystallization interface $D\partial C/\partial n = v_c(1 - k_0)C \cos\theta$, where \mathbf{n} is the normal direction, v_c is the crystal pulling rate, and θ is the angle between the xy (horizontal) plane and the interface normal vector.

b. On the melt free surface, due to the assumption of homogeneous concentration distribution in the argon atmosphere, a fixed concentration is applied normalized to $C = 1$.

c. At the melting interface – a ring-shaped profile, where the dopant concentration at the ring is equal to the concentration on the free surface, and the silicon feed rod is considered pure ($C = 0$).

2. Calculation results. Phase boundaries of the considered 4" FZ system with the crystal pulling rate $v_c = 3.4$ mm/min (detailed information about the system parameters and inductor geometry can be found in [5]) were calculated using the program FZone and shown in Fig. 3, left. When the EM correction is included, a higher inductor current I_0 is required to hold the prescribed zone height (32.5 mm) and this leads to a larger deflection of the crystallization interface H_c (see Table 1). This shape is closer to the experimental one. The induced EM power density and the force vectors for a different inductor current frequency are shown in Fig. 3, right. Heat sources were approximately the same, because the calculation algorithm maintained the fixed zone height. F_{EM} was significantly different: maximum values were 0.49 N/m² for 3 MHz and 0.70 N/m² for 2 MHz.

Using the obtained axisymmetric shape of the phase boundaries, 3D HD calculations were performed on a block-structured mesh consisting of 80 000 hexahedral

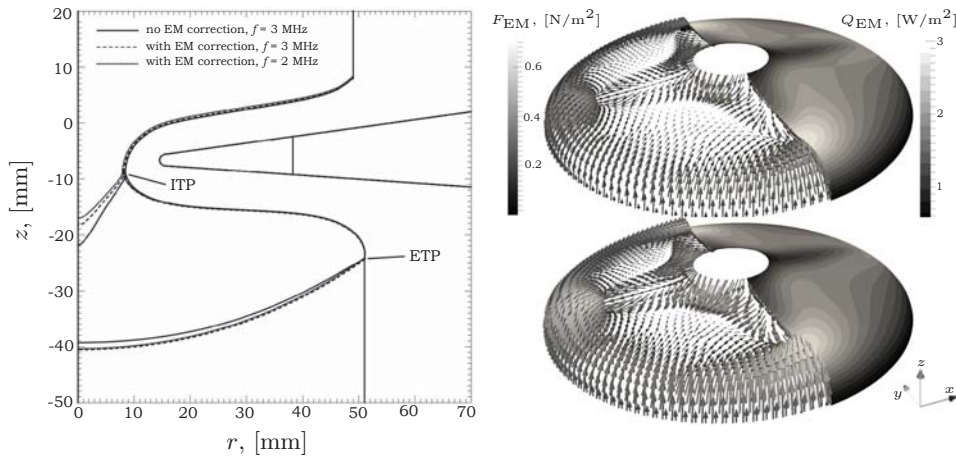


Fig. 3. Left: phase boundaries of the considered system for various EM fields. Also shown are the ETP and ITP. Right: EM heat sources and EM force on the melt free surface for cases with the EM correction for a different inductor current frequency (top – 3 MHz, bottom – 2 MHz). Current inlets are located in the positive direction of the x -axis.

Table 1. Results of phase boundary calculations.

Case	I_0 , [A]	H_c , [mm]
No EM correction, $f_{ind} = 3$ MHz	870	15.0
With EM correction, $f_{ind} = 3$ MHz	884	16.2
With EM correction, $f_{ind} = 2$,MHz	953	16.3

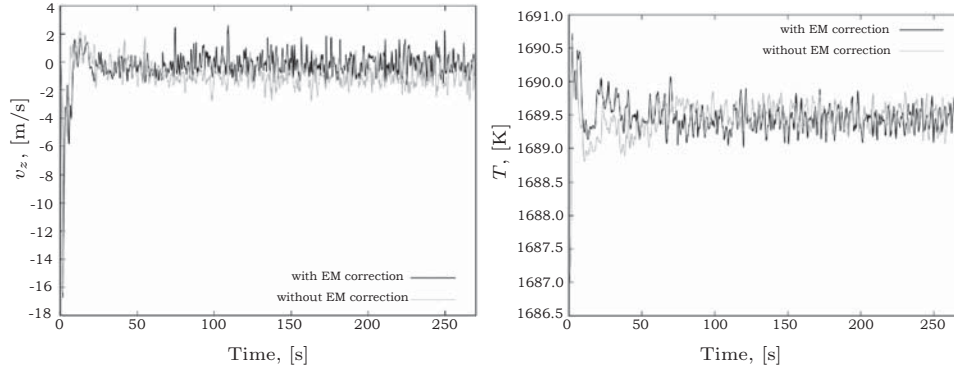


Fig. 4. Oscillations of the melt velocity vertical component (left) and temperature (right) at the probe point located 1 mm above the crystallization interface at $x = 0$ and $y = 25$ mm.

elements. As a result, non-stationary physical fields were obtained. Nevertheless, the phase boundaries were fixed, so transient behaviour and control of the FZ control process was not considered in these calculations, and unsteady behaviour can be expressed only in characteristic oscillations. The melt velocity and temperature oscillations at a particular probe point near the crystallization interface are shown in Fig. 4. An approximate oscillation period was the same for both fields, about 2–3 s. As there were no qualitative differences between the cases with and without EM correction, it can be concluded that the use of correction does not significantly change the time-dependent behaviour of the present numerical model.

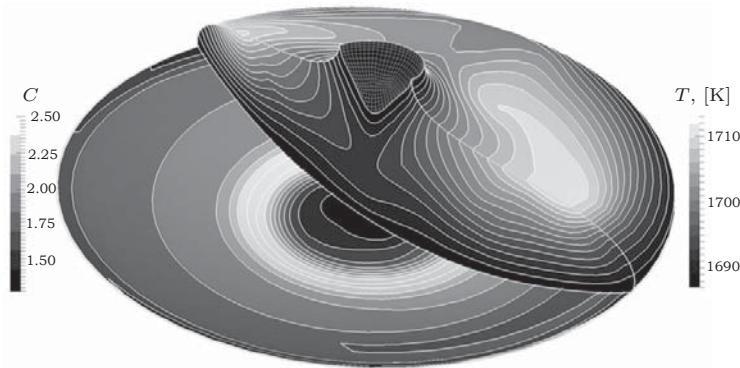


Fig. 5. Crystallization interface and vertical cut of the melt. The melt temperature is shown in the right part of the melt; dopant concentration is depicted at the crystallization interface. At the melting interface mesh edges are shown. A calculation example with the EM correction and $f_{ind} = 3$ MHz.

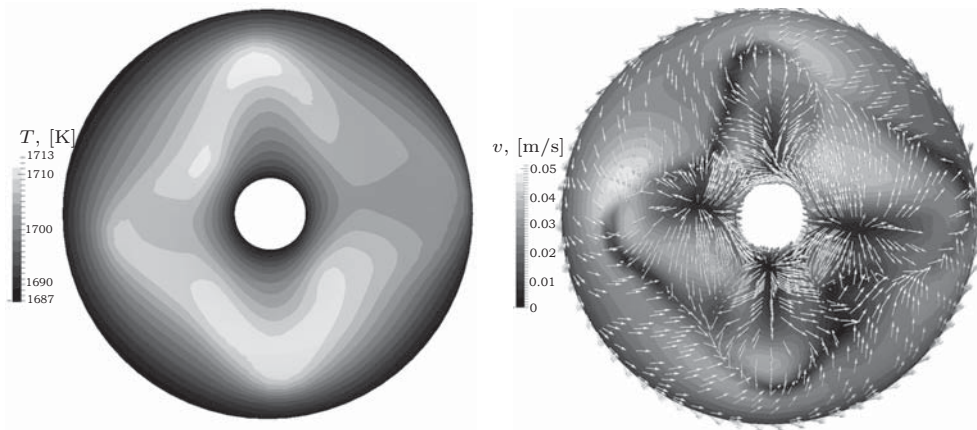


Fig. 6. Top view of the melt free surface with temperature (left) and velocity (right). A calculation example with the EM correction and $f_{\text{ind}} = 3$ MHz.

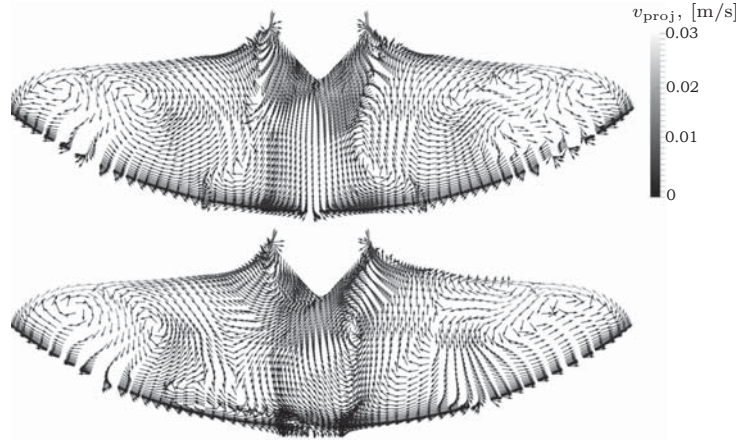


Fig. 7. Time-averaged melt velocity projection on the vertical slice of the melt, perpendicular to inductor current suppliers. Top: $f_{\text{ind}} = 3$ MHz, bottom: $f_{\text{ind}} = 2$ MHz.

An example of the calculated fields, averaged over a 5 s interval at the end of HD calculations – melt velocity, temperature and dopant concentration – is illustrated in Figs. 5, 6 and 7. Two characteristic temperature maxima on the melt free surface are formed below the additional slits of the inductor due to non-symmetric induced heat sources (see Fig. 3). Therefore, the lowest temperature occurs below the main slit of the inductor.

The velocity field in the vertical slice of the melt (see Fig. 7) shows that near the ETP the electromagnetic forces dominate and create a distinct vortex. As it frequently happens in the 4" FZ system, a dopant concentration maximum is formed by two vortices swirled in opposite directions: the first one occurs due to the melt vertical motion from the crystallization interface and the second is created by the EM force on the free surface. When the inductor frequency is decreased to 2 MHz, the velocity field in the considered vertical slice becomes more asymmetric and less stable (i.e. stronger fluctuations in time), which leads to more intensive mixing processes. On the other hand, the top view of the free surface shows a distinct asymmetry of the velocity field (see Fig. 6). It means that the melt velocity in the vertical slice can only partially represent the processes in the whole melt.

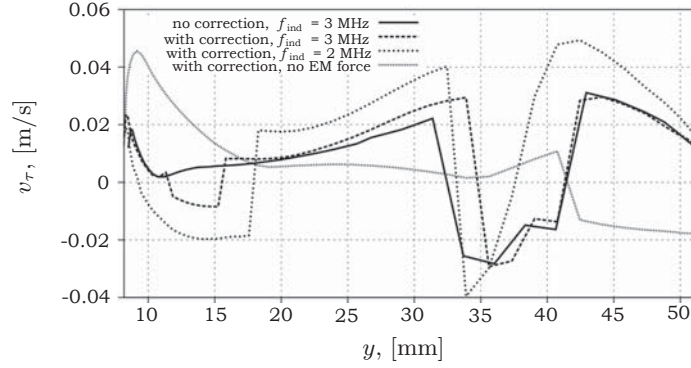


Fig. 8. Distribution of in-plane velocity on the melt free surface; y is a horizontal coordinate perpendicular to inductor current suppliers; 51 mm corresponds to the ETP; v_τ is defined as positive if the melt moves towards the crystal axis.

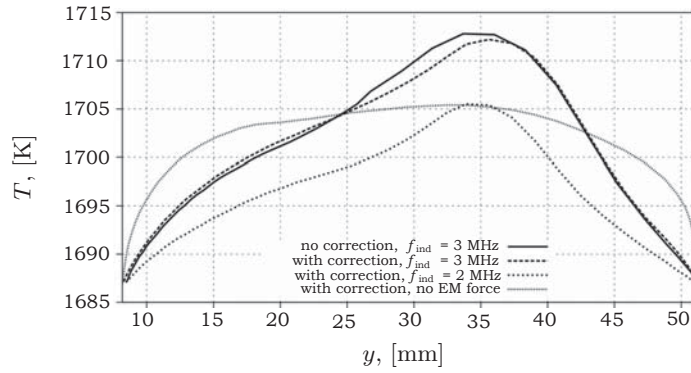


Fig. 9. Distribution of temperature on the melt free surface; y is a horizontal coordinate perpendicular to inductor current suppliers, 51 mm corresponds to the ETP.

To investigate the influence of EM forces on the melt motion more precisely, the distribution of the tangential melt velocity component (projected on the plane of the slice) is shown in Fig. 8. As the EM force increases with the lower inductor frequency, the melt velocity considerably increases. Both near the ETP and near the ITP (for definition, see Fig. 3) the melt flow becomes stronger in the direction from lower to higher temperatures. It means that for the lower inductor frequency, the EM force is stronger than the Marangoni force, excluding a very small region near the ITP. Moreover, the temperature profile on the free surface (see Fig. 9) indicates a more intense mixing in the melt, which leads to low temperature gradients and low Marangoni force.

One more important process is the reverse of the vortex in the vicinity of the ETP when EM forces are turned off. In Fig. 8 it can be seen that the tangential velocity component varies from positive to negative, and this direction corresponds to the direction of Marangoni convection – from higher to lower temperatures. This tendency is very pronounced in the vicinity of the ITP, too.

Finally, from the concentration distribution at the crystallization interface, RRV profiles were obtained (see Fig. 10). Table 2 which summarizes the squared differences between experimental and calculated RRV profiles, shows that the case with the EM correction and $f_{\text{ind}} = 3$ MHz describes the experimental data more precisely than others. Experimental data was obtained using $f_{\text{ind}} = 3$ MHz, and the expected result that the calculation with $f_{\text{ind}} = 2$ MHz has a significantly worse

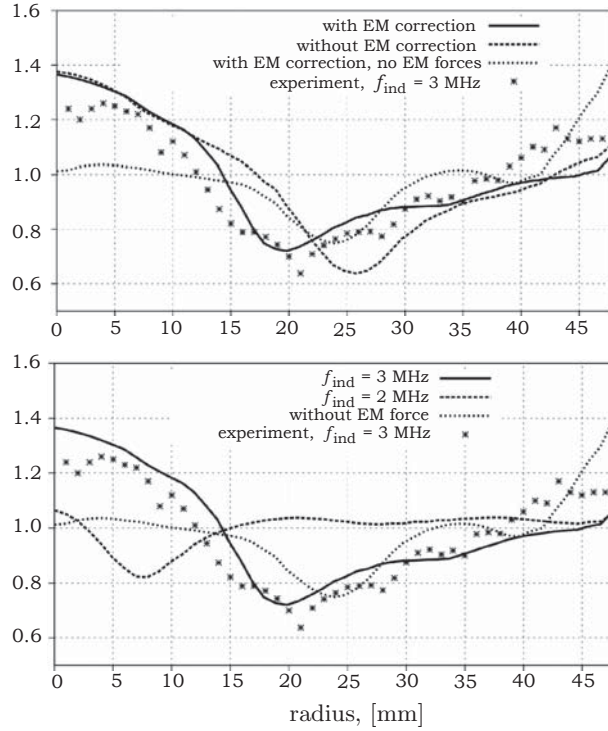


Fig. 10. RRV profiles. Resistivity is normalized to its average and displayed in arbitrary units. Top: $f_{ind} = 3$ MHz. Bottom: calculations on the mesh obtained with the EM correction.

Table 2. Sum of squared differences (deviations) between experimental (obtained with $f_{ind} = 3$ MHz) and calculated RRV profiles, in arbitrary units.

No EM correction, $f_{ind} = 3$ MHz	0.80
With EM correction, $f_{ind} = 3$ MHz	0.38
With EM correction, no EM forces	0.88
With EM correction, $f_{ind} = 2$ MHz	2.11

agreement with experiment indicates that the used system of numerical models is sensitive to the inductor current frequency. For $f_{ind} = 2$ MHz, the resistivity minimum was shifted towards the crystal axis due to the changed structure of vortices, and the whole profile became flatter due to a more intense convection in the melt (see Fig. 7). It can be concluded that the RRV profiles are very sensitive to the changes in melt flow, so that they can respond even to small velocity differences and can be used to verify the EM correction and other possible improvements in boundary conditions and calculation process.

3. Conclusions. It has been shown that the EM field has a significant influence both on the shape of phase boundaries and on the melt hydrodynamics. The EM correction allows to describe phase boundaries more precisely, and this leads to changes in RRV profile, even although the influence of the correction is considered only through the change of phase boundaries, not including it in temperature boundary conditions for 3D melt flow calculations. The position of resistivity minima became closer to the experimentally observed ones and the sum

of squared differences diminished, therefore, the EM correction has improved the models qualitative and quantitative correspondence to experiment.

When calculations are performed without EM forces, the distribution of velocity on the melt free surface shows that the Marangoni force reverses vortices near the ETP and an additional resistivity minimum occurs. Clear influence of the decrease of the inductor current frequency was detected due to the significant increment of EM forces: the resistivity minimum shifted towards the crystal axis and the RRV profile became flatter. The next aim of the study could be the implementation of EM correction in a 3D HF EM calculation program, which creates EM heat sources – boundary conditions for melt flow calculations, to observe direct influence of the EM correction on the 3D melt flow and dopant distribution. One more possibility is to use the correction not only for heat sources, but also for the EM force distribution.

Acknowledgments. This work is supported by the European Regional Development Fund, project contract no. 2013/0051/2DP/2.1.1.1.0/13/APIA/VIAA/009.

REFERENCES

- [1] K. LĀCIS, A. MUIŽNIEKS, A. RUDEVĪČS, A. SABANSKIS. Influence of DC and AC magnetic fields on melt motion in FZ large Si crystal growth. *Magnetohydrodynamics*, vol. 46 (2010), no. 2, pp. 199–218.
- [2] H.-J. ROST, R. MENZEL, A. LUEDGE, H. RIEMANN. FZ silicon crystal growth at reduced RF frequencies. *J. Crystal Growth*, vol. 360 (2012), pp. 43–46.
- [3] G. RATNIEKS, A. MUIŽNIEKS, A. MUHLBAUER. Modelling of phase boundaries for large industrial FZ silicon crystal growth with the needle-eye technique. *J. Crystal Growth*, vol. 255 (2003), pp. 227–240.
- [4] A. MUIŽNIEKS, A. RUDEVĪČS, H. RIEMANN, U. LĀCIS. Comparison between 2D and 3D modelling of HF electromagnetic field in FZ silicon crystal growth process. *Proc. International Scientific Colloquium Modelling for Material Processing* (Riga, 2010), pp. 61–65.
- [5] K. SUROVOVS, A. MUIŽNIEKS, A. SABANSKIS, J. VIRBULIS. Hydrodynamical aspects of the floating zone silicon crystal growth process. *J. Crystal Growth*, vol. 401 (2014), pp. 120–123.

Received 09.02.2015